II   LAURA (*L-Band AUtomatic RAdiometer*) instrument. Introduction

This chapter presents a description of the LAURA instrument, composed by two Dicke radiometers (DR) and a Digital Correlator Unit (DCU). The LAURA radiometer is thermally controlled. It is mounted inside a plastic (high molecular weight polythene) box inside covered with a metal film to prevent radio frequency interferences, and several inner layers of polystyrene to preserve the instrument from the external humidity and to isolate it from external temperature changes. The LAURA instrument is mounted on a pedestal to perform elevation and/or azimuth scans in an automatic manner. Radiometric, temperature, position and orientation data are acquired together with meteorological data and video imagery using an industrial PC (designed for rough environments) running a control software developed by UPC.

II.1   LAURA radiometer. Radiometer description

The LAURA radiometer (Figure 2.1) is composed of two Dicke radiometers, for the horizontal and vertical polarizations (T_H and T_V) and a complex correlation radiometer for the third and fourth *Stokes* parameters (U, V). LAURA's antenna is composed by an array of 4x4 dual-polarization microstrip patches with 20º half-power beamwidth, 95.2 % main beam efficiency at side lobe level, and cross-polarization level better than – 35 dB in the whole pattern, and better than – 40 dB in the main beam.
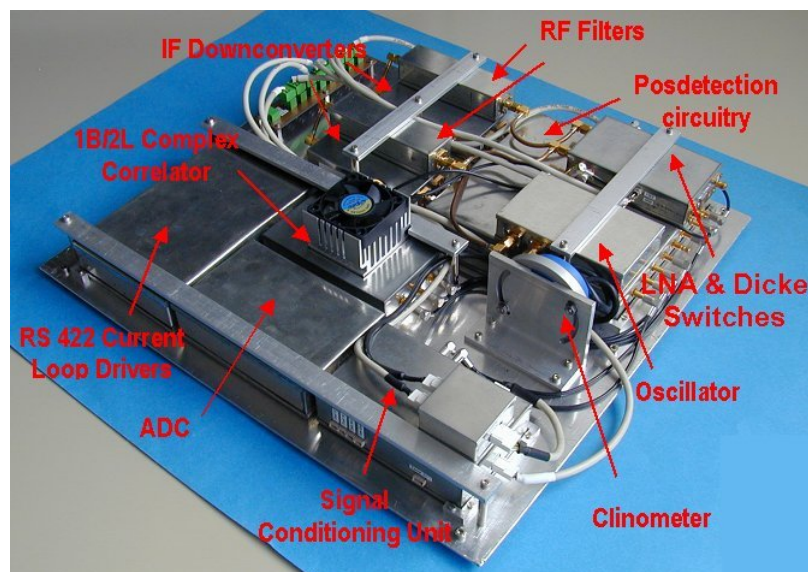

Figure 2.1. LAURA electronics [3].

The receiver architecture is based on 2 L-band receivers with I/Q down-conversion, whose inputs can be switched between: i) the H/V antenna ports, ii) two independent matched loads for each channel, or iii) a common noise source. The in-phase components of both channels are connected to two power detectors. The Dicke radiometers (T_H and T_V) are formed by switching receivers' inputs from positions (i) and (ii) at 122 Hz, and performing a synchronous demodulation. The third and fourth Stokes parameters (U and V) are measured with a complex 1 bit-2 level digital correlator. LAURA's schematic receiver block diagram is shown in Figure 2.2.
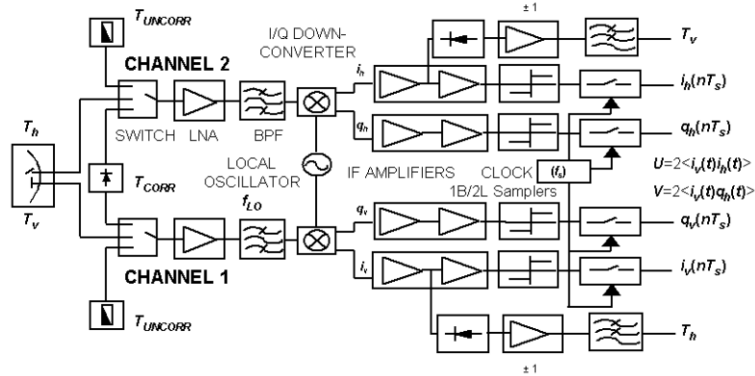
Figure 2.2. Block diagram of LAURA [3].

II.1.1 Dicke radiometer

Figure 2.3 shows a block diagram of a Dicke radiometer (DR). A DR it is essentially a total power radiometer, that it is composed by an antenna connected to a super-heterodyne receiver of bandwidth B and total power gain G_s, followed by a quadratic detector and a low-pass filter with two additional features: i) a switch -usually known as the Dicke switch- that is connected to the antenna's output or a matched load, and to the receiver's input, and ii) a synchronous detector placed between the square-law detector and the low-pass filter (integrator).
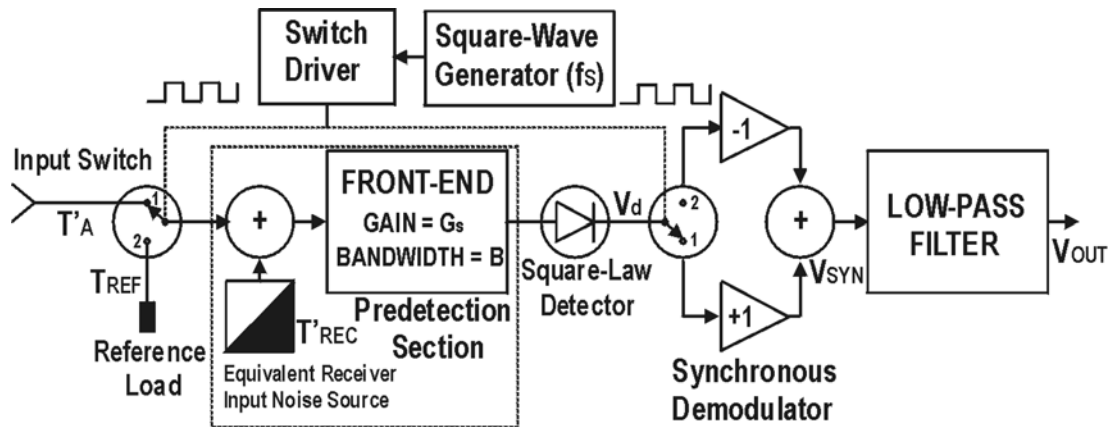

Figure 2.3. Functional block diagram of a DR [1].

The working principle is based on a differential measurement. First, the input is switched between the antenna (apparent temperature T_{AP}) during half cycle, and a constant reference noise source, during the second half cycle, at a switching rate f_s. Second, in synchronism with the input Dicke switch, a synchronous demodulator switches between two unity-gain amplifiers, with opposite polarity (+1 and –1). The unity-gain amplifier outputs are then summed, and low-pass filtered (integrator) with time constant 2τ, being τ the integration time. The radiometer's output voltage is given by [1]:

$$\overline{V_{out}} = \frac{1}{2} \cdot G_s \cdot \left(T_A - T_{ref} \right) \ ,$$

(2.1)

where G_S is the average system power gain, and is expressed as:

$$G_s = k \cdot B \cdot G \cdot C_d \; , \tag{2.2}$$

and C_d is the detector constant, T_A is the antenna temperature, and T_{ref} is the reference-source noise temperature.

The system temperature (T_{SYS}) is defined as the sum of T_A and the receiver noise temperature (T_{REC}). On the other hand, the radiometric sensitivity ΔT is the minimum change in T_{SYS} that is necessary to produce a detectable change at the radiometer's output and it is equal to the square root of the quadratic sum of the gain variations, the noise variations due to T_A and T_{ref} (during half-cycle each one), and T_{REC}. Hence, ΔT is given by [1]:

$$\Delta T = \left[\frac{2 \cdot (T_A + T_{REC})^2 + 2 \cdot (T_{ref} + T_{REC})^2}{B \cdot \tau} + \left(\frac{\Delta G_s}{G_s} \right)^2 \cdot (T_A - T_{ref})^2 \right]^{\frac{1}{2}} , \tag{2.3}$$

where ΔG_s is the rms value of the detected power gain variations (ac component). If T_A and T_{ref} are the same, the receiver gain fluctuations do not contribute to the radiometric sensitivity. In this situation the Dicke radiometer is "balanced," and ΔT reduces to:

$$\Delta T = \frac{2 \cdot (T_A + T_{REC})}{\sqrt{B \cdot \tau}} \; , \tag{2.4}$$

II.1.1.1 The antenna

The electrical parameters that are necessary to take into account in the LAURA antenna design are: the directivity (or half-power beamwidth), the Main Beam Efficiency (η_{MBE}), the cross-polarization ratio, the antenna matching, and the ohmic losses (η_l), as well as other mechanical parameters such as weight and physical dimensions. LAURA antenna was designed specifically for this application. According to the first chapter, the T_B sensitivity at SSS is maximum at L-band therefore the antenna's weight and size are two of the main restrictions into this design. As LAURA receiver is a fully polarimetric radiometer, the four Stokes parameters must be measured, and therefore the antenna's cross-polarization level must be very low. The LAURA antenna's directivity depends mainly on the desired angular resolution and main beam efficiency. The main beam efficiency η_{MBE} is also a critical design parameter in a radiometer. It is defined as the ratio between the energy received by the main beam and the total energy received by the antenna (main beam + all sidelobes). The power collected at the antenna output T_A' can be expressed as:

$$T_A' = \eta_r \cdot \left[\eta_{MBE} \cdot T_{MBE} + (1 - \eta_{MBE}) \cdot T_{SL} \right] + (1 - \eta_r) \cdot T_o \; , \tag{2.5}$$

which is different from T_{MBE}.

In eqn. (2.5), T_{MBE}, T_{SL} and T_o are the main beam apparent temperature, the side lobes apparent temperature, and the antenna physical temperature respectively. To illustrate this problem, the situation presented in Figure 2.4 can be considered.
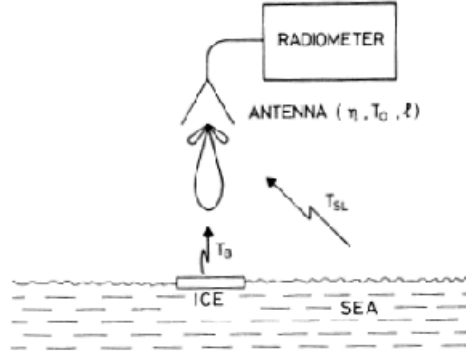

Figure 2.4. Importance of high antenna main beam efficiency: antenna measuring an ice floe [4, p 83].

To illustrate the importance of the antenna's η_{MBE}, two apparent close values of the main beam efficiency are considered. First of all, an antenna with η_{MBE} = 90 % senses an ice floe on the surface of the sea. The ice floe is just the size of the area on the ground illuminated by the main beam. Assuming typical values - T_{MBE} (ice) = 270 K and T_{SL} (sea) = 100 K, and no ohmic losses (η_r = 0), the measured T_A' is 253 K, that is 17 K lower than the value which should be measured. Secondly, if an η_{MBE} = 95 % is assumed for the same antenna and for the same conditions, the measured T_A' is 262 K. Finally, assuming an η_r = 95 % and T_o = 298 K, the measured T_A' is 263.7 K. Moreover according to (2.5), and to avoid the T_A physical temperature dependence, the antenna losses should be as small as possible, and the antenna physical temperature as constant as possible.

A picture of LAURA's antenna is shown in Figure 2.5a. The radiating element Figure 2.5b is a coaxial-fed array of 4x4 microstrip patches (0.7 m inside). The 4x4 patches, (~ 9 cm side) are printed on a 0.8 mm-thick fiberglass circuit board, separated 0.75 λ (160 mm) one from the other, and at the appropriate distance (~ 1 cm) over a ground plane to achieve the required bandwitdh. The dielectric between the patch and the ground plane is air to minimize the ohmic losses. Figure 2.6a and Figure 2.6b show a picture of the feed network at one polarization and the antenna connection network. To avoid the noise generated by the resistors of Wilkinson power splitters, the feed network is based on non-resistive dividers (Figure 2.6a). The specifications of the antenna are: relatively narrow beamwidth (< 20º), high η_{MBE} (>95%) to minimize contributions from secondary lobes, and very low cross-polar level (- 35 dB). A horn antenna could also be used for this purpose, but due to the dimensions, weight, motion requirements as well as to be able to have the antenna thermally controlled, an array of microstrip patches was the preferred option. The co-polar and cross-polar antenna radiation patterns are shown in Figure 2.7, and their cuts in Figure 2.8a to Figure 2.8c. The main beam efficiency is represented in Figure 2.8d as a function off-bore sight angle. At side lobe level (θ = 22°) the η_{MBE} = 95.2 %. The triangular illumination,

(weighs {1:2:2:1}) achieves a side lobe level of -18 dB in the E-plane and - 26 dB in the H-plane. Antenna, cable losses and isolators are 0.55 dB in each channel. LAURA's antenna match is better than -10 dB at 1.4135 GHz, (including the feed network). The match from a single patch is better than –15 dB. Two isolators are placed between the front-end and the antenna to minimize the mismatches. Their measured scattering parameters are summarized in Table 2.1.

Table 2.1. Isolators characterization at f_o =1.4135 GHz

Polarization	$\left|S_{11}\right|^2$	$\left|S_{12}\right|^2$	$\left|S_{21}\right|^2$	$\left|S_{22}\right|^2$
H isolator	-17.92 dB	-22.43 dB	-0.30 dB	-17.95 dB
V isolator	-17.18 dB	-21.03 dB	-0.37 dB	-15.61 dB

(a)   (b)
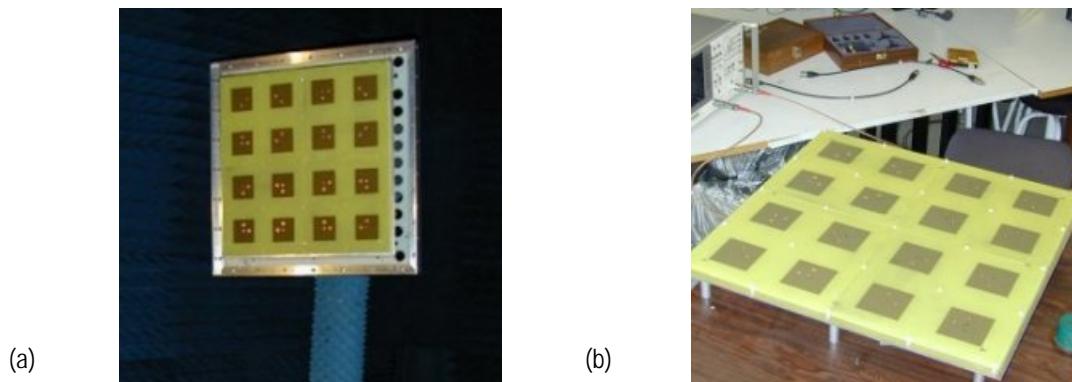
Figure 2.5. (a) Antenna aspect, and (b) radiating element.

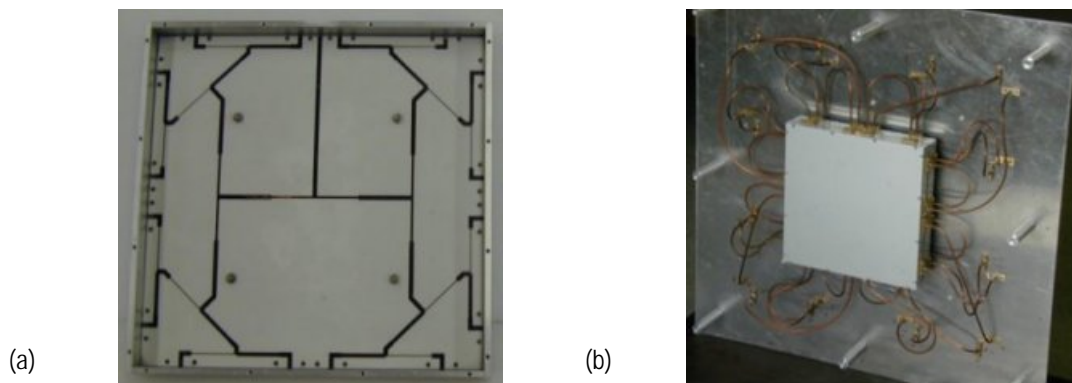(a)   (b)

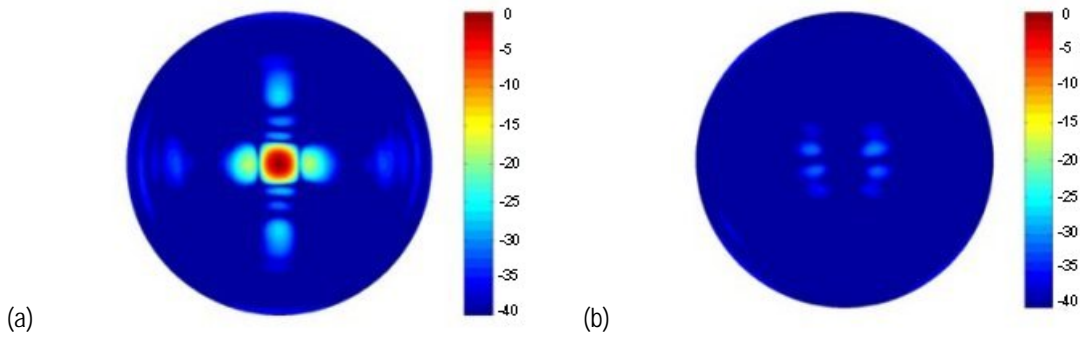Figure 2.6. (a) Feed network, and (b) antenna's rear view.

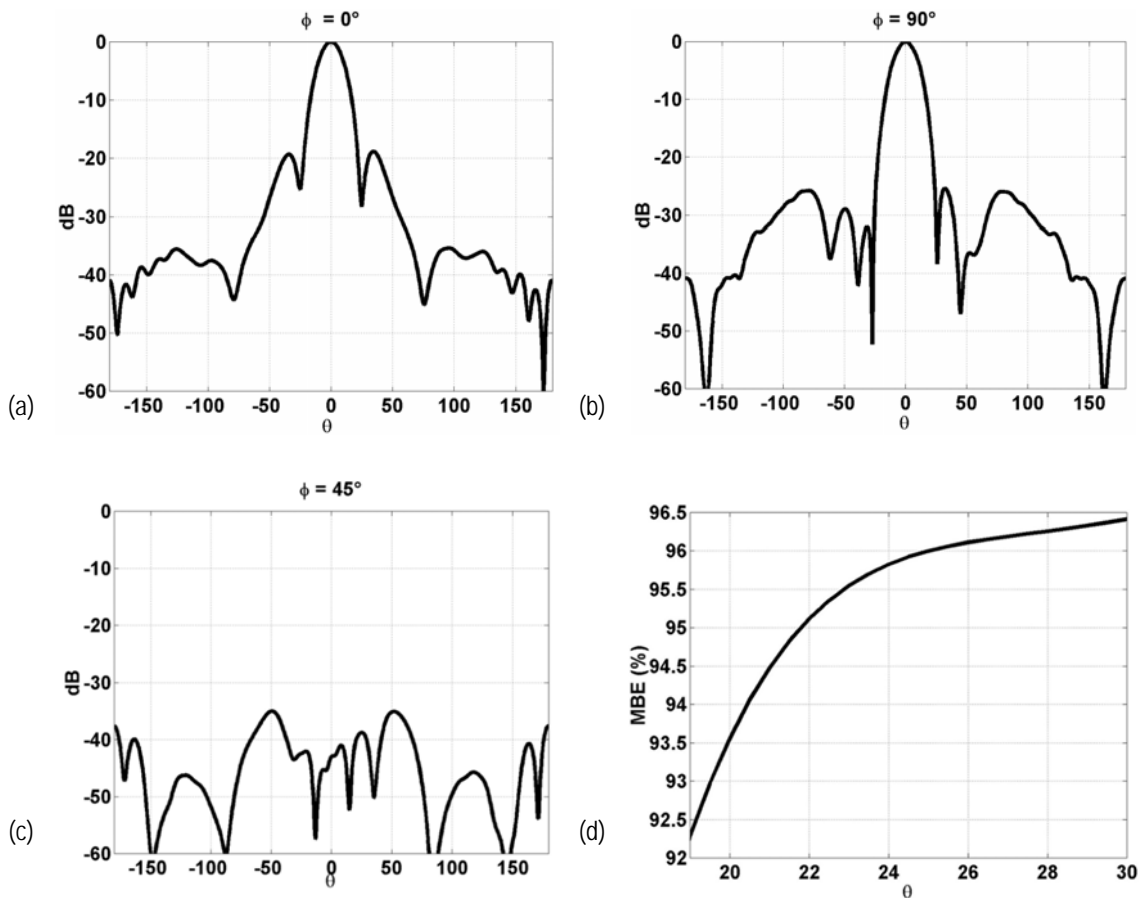Figure 2.7. Normalized antenna radiation pattern, (a) co-polar, and (b) cross-polar.

Figure 2.8.(a) co-polar cut at E plane, (b) co-polar cut at H plane, (c) cross-polar cut at 45°, and (d) Main Beam Efficiency computed from 0º to θ, and ϕ from 0° to 360°. Secondary lobe level at $\theta = 22°$.

II.1.1.2 Dicke switch and Low noise amplifier (LNA)

The Dicke switches, the LNAs, the control logic, and the correlated noise source are mounted into the first block. The LNA is a MAX2640 transistor with 15 dB gain, and 0.8 dB noise factor. Two cascaded switches (total isolation = 48 dB) are used to switch the antenna port (H- and V- channels) and the matched load during the measurements. The other three switches are used to calibrate the correlator's offset and the phase. The offset calibration is made by injecting uncorrelated noise from the two matched

loads. Phase calibration is achieved by injecting correlated noise to both channels simultaneously. The correlated noise is generated from a match load, amplified by a MINICIRCUITS MAR-6 amplifier, and divided by a BPG2 power splitter (isolation = 28 dB, and insertion loss = 0.6 dB). The control logic (Table 2.2) is in charge of generating the necessary signals to control the RSW-2-25p switches in these three situations: (i) normal measurements, (ii) offset, and (iii) phase calibrations. In mode (i) the CLOCK signal (122 Hz) attacks the Dicke switches (L2 = CLOCK), and the other three switches are closed simultaneously (L1 = 0). To calibrate offset (ii), the Dicke switches are unconnected from the H- and V- channels antenna ports, (L2 = 0) and the other three switches are closed (L1 = 0), because the correlated noise injection (CNI) control signal is equal to 0. The last case (iii) is the same as (ii), but CNI = 1 and L1 = 1. The electric schematic is shown in Figure 2.9. The input and output LNA matching networks, are the stubs presented in Figure 2.10 a and Table 2.3. The substrate circuit is RO4003 with a dielectric constant of ε_r = 3.3, and thickness = 0.813 mm [5]. The noise factor of the LNA block presented in the Figure 2.10b is 1.34 dB (H- channel) and 1.42 dB (V- channel) at f_o = 1,4135 GHz including the switch insertion losses. Its gain is 15.7 dB (H- channel) and 14.7 dB (V- channel).
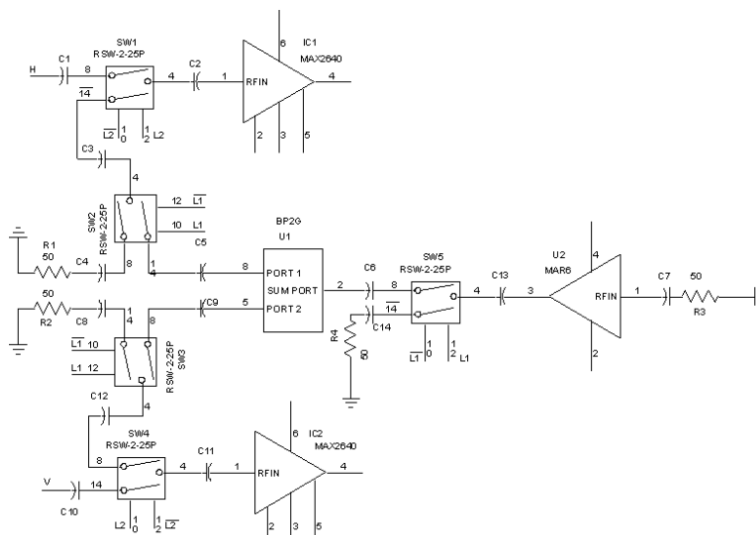

Figure 2.9. Switch's circuitry, [6].

Table 2.2. Control logic. Function table.

Inputs		Outputs	
Correlated/Uncorrelated noise (CNI)	Measurement/ Calibration (Meas)	L1	L2
0	0	0	0
0	1	0	CLOCK
1	0	1	0
1	1	0	CLOCK

Table 2.3. Specifications of LNA stubs.

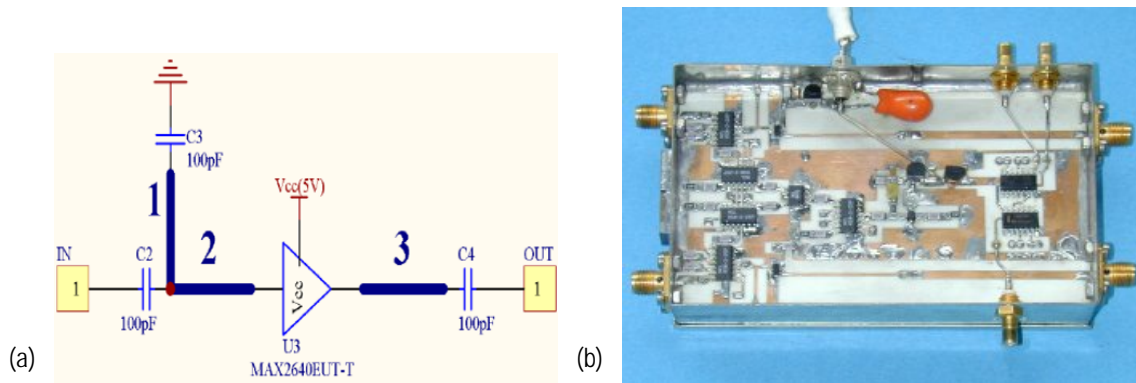| Stub number	Impedance	Width	Length
1	95 Ω	0.549 mm	8.826 mm
2	95 Ω	0.549 mm	2.829 mm
3	97.46 Ω	0.526 mm	27.310 mm

Figure 2.10. (a) MAX2640 matched network [5], and (b) Dicke switch and LNA.

II.1.1.3   Band-pass filter

To measure the power collected by the radiometer at each polarization and minimize the out-of-band radiation, a selective band-pass filter centered at 1.4135 GHz – spectral band reserved for passive observation - is needed. The band-pass filters were designed by UPC with a new topology of λ/4 short-circuited resonators [7] instead of using the traditional λ/2 open circuit coupled lines to reduce its physical size. A picture of the filters is shown in Figure 2.11, and the frequency response is presented in Figure 2.12a and Figure 2.12b. The half-power filter bandwidth is approximately 50 MHz. Frequency response is finally shaped after I/Q down-conversion. Return and insertion losses are summarized in Table 2.4.

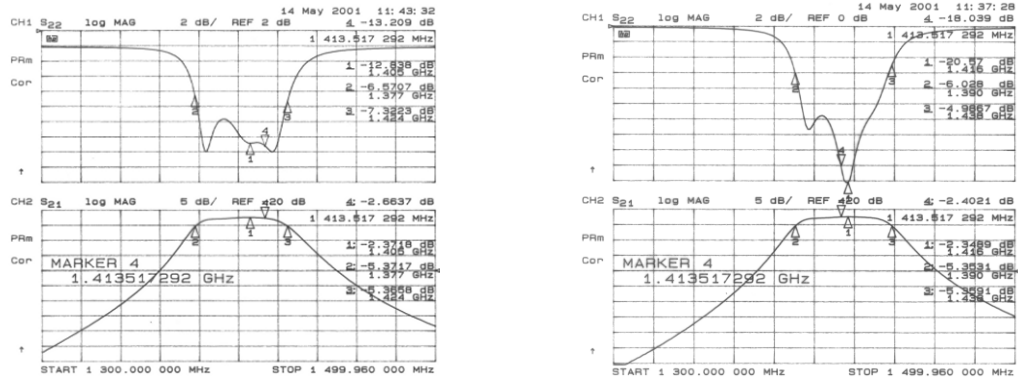

Figure 2.11. Band pass filters [7].

(a)   (b)

Figure 2.12. Filter's insertion loss and frequency response, (a) H‑channel, and (b) V‑channel.

Table 2.4. RF band pass filter insertion and return loss at f_0 = 1.4135 GHz

	Return loss	Insertion loss
H‑channel	-13.21 dB	-2.66 dB
V‑channel	-18.04 dB	-2.40 dB

II.1.1.4 I/Q Demodulator

The H‑ and V‑ polarization band-pass filtered signals have a power of –85 dBm approximately. They must be converted to baseband, using a down-converter for each channel (Figure 2.13a). A direct conversion has been selected, because of the simpler and cheaper circuitry in front of a heterodyne receiver. The input signals are first amplified by two MAR-6 amplifiers (with 14 dB gain each at 1.4135 GHz Figure 2.13b) to attack the MAX2102 down-converters at a – 55 dBm level. The Maxim's MAX2102 integrated circuit input ranges are between – 69 dBm to –19 dBm, providing an in-phase and quadrature outputs of 500 mV$_{pp}$ over 100Ω.

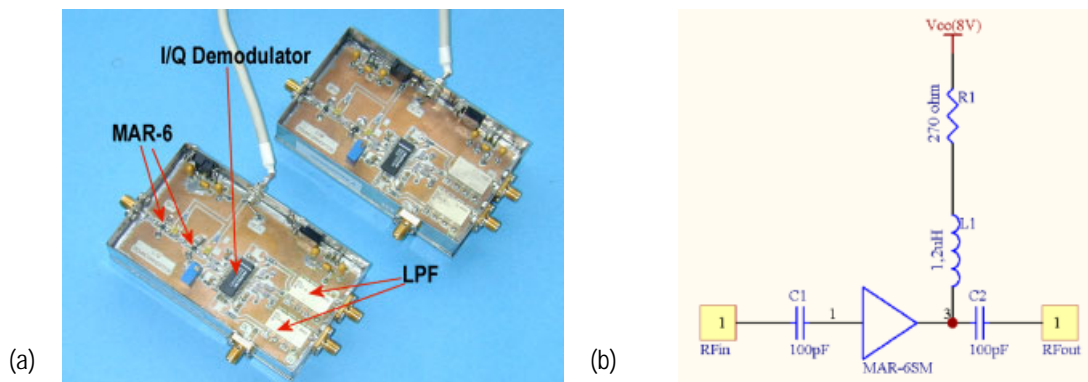(a)   (b)

Figure 2.13. (a) Down-convert modules (H‑ and V‑ channel), and (b) MAR-6 SM connection, [5].

The MAX2102 is composed by: a low noise amplifier plus an AGC, two mixers, a 90° phase shifter, offset correctors, and I/Q amplifiers. The output signal can be adjusted using a variable resistor (10 KΩ). The local oscillator signal level is between – 15 dBm and – 5 dBm. At its output, a low-pass filter (50 Ω

input impedance) is used to suppress harmonics, and effectively set the band-pass bandwidth to 16 MHz. A 50 Ω resistor is needed at the filter's input to match the MAX2102's output.

The total power consumption of each down-convert block, including the two MAR-6 amplifiers is 120 mA. The overall frequency response of the two channels, is represented in Figure 2.14a, (H- channel) and Figure 2.14b, (V- channel).
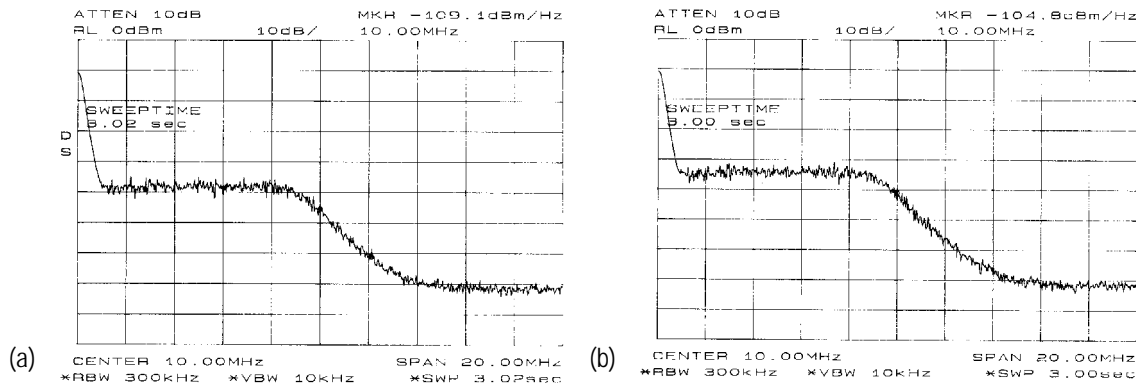

Figure 2.14. Frequency response of the downconverter measured with noise thermal, a) H- and b) V- channel.

II.1.1.5 Local oscillator (LO)

The local oscillator [8] is shown in Figure 2.15a. Since LO phase stability is critical, a PLL was mounted using the UMA1021M programmable frequency as a phase comparator. A stable external 20 MHz clock reference was generated and injected in the phase comparator. Finally the VCO was implemented using discrete components. The central frequency is 1.413 GHz and the RF power –11 dBm. A MAR-6 amplifier is used amplify the LO that, once splitted, attacks the down-converters of the H- and V- channels. Phase noise is about – 84 dB at 10KHz, (Figure 2.15b).
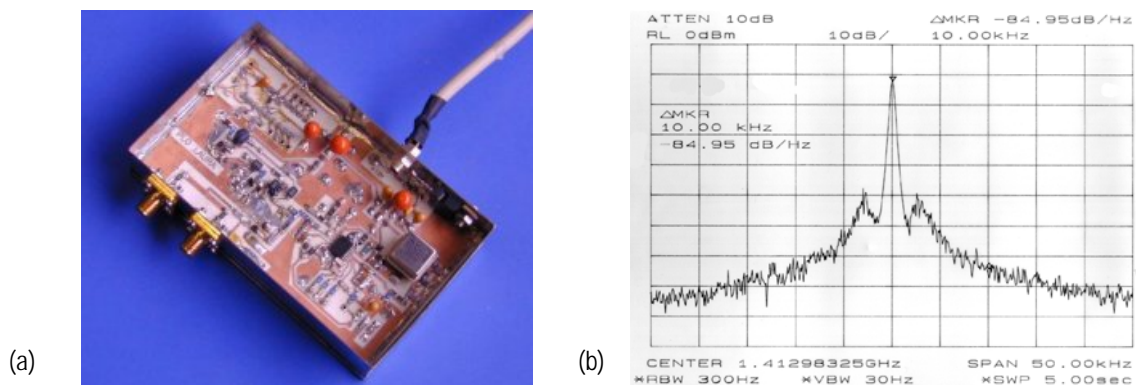

Figure 2.15. (a) Local oscillator, and (b) its phase noise.

II.1.1.6 Resistive divider

A frequency synthesizer is an alternative option to guarantee a pure tone to be used as LO. In this case, it is necessary only a power splitter, to attack the downconverters of both channels. The picture of the resistive power splitter designed is shown in Figure 2.16. To compensate the 6 dB power splitter

losses, and those of the 20 m long cable from the synthesizer in the radiometer control rack to the radiometer, a MAR-6 is mounted at each channels' output.
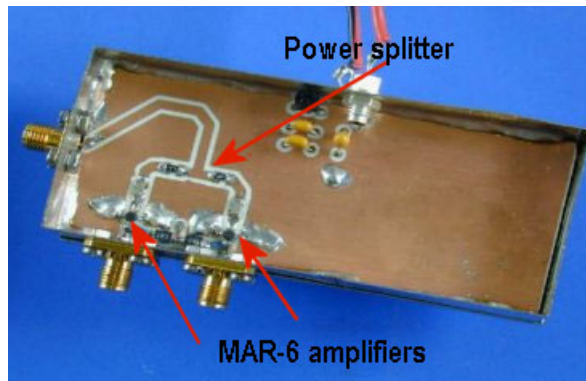

Figure 2.16. Resistive power splitter.

II.1.1.7 Post-detection circuit

The power detection module is shown in Figure 2.17a and Figure 2.17b. This module [9] is divided into six different blocks.
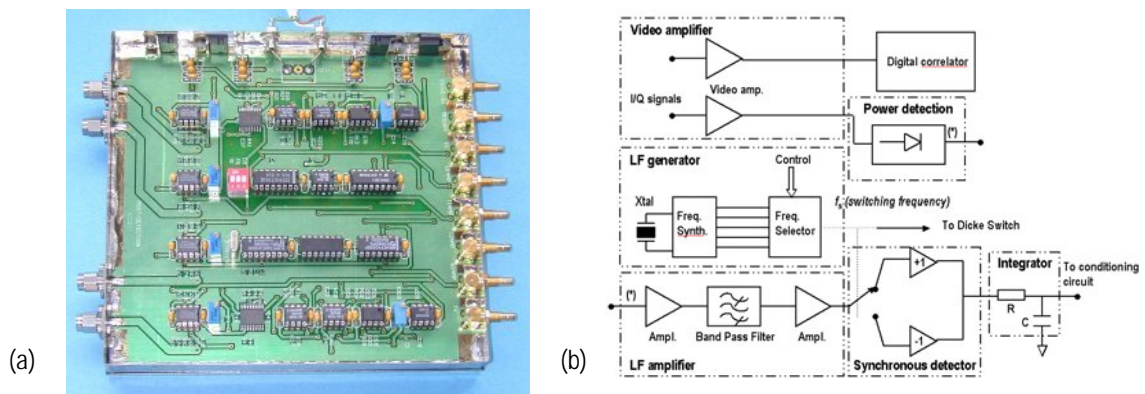

(a)   (b)

Figure 2.17. Post-detection circuit, (a) picture, and (b) block diagram.

- The video amplifiers to attack the digital correlator samplers with the correct signal levels,

- The power detection module composed of two Dicke detectors to measure the first and the second Stokes parameters (T_H and T_V),

- The control logic to generate asynchronous measure/calibration signals, and the injection of correlated/ uncorrelated noise (Figure 2.9),

- The LF amplifiers to amplify the signal level to a maximum range so as to get the maximum sensitivity (V/K) at the Dicke radiometer output,

- The modulator-demodulator clock's signal, and

- The integrator (low pass filter).

The I/Q signals of the two channels (H- channel, V- channel) are connected to four NE592 differential gain adjustable video amplifiers. The NE592's output power level is adjusted to 0 dBm. One of the NE592's outputs is connected to the digital correlator, and the other one, attenuated 25 dB, and connected to the power detector (Figure 2.18). The MACOM's MA4CS102E diodes are selected to detect the I/Q power of the two channels. It consists of a differential detector composed by two diodes, one of them connected to the I/Q signals and the other one to ground. The main goal of the differential configuration chosen is to cancel the temperature drifts that contribute in the same way to both diodes (D1, D2), using an INA114 instrumentation amplifier (Figure 2.19a). The best linearity of the MA4CS102E diodes is achieved in the range from − 28 dBm to − 22 dBm (Figure 2.19b). In this range, the absolute linearity error is always smaller than 0.7 %.
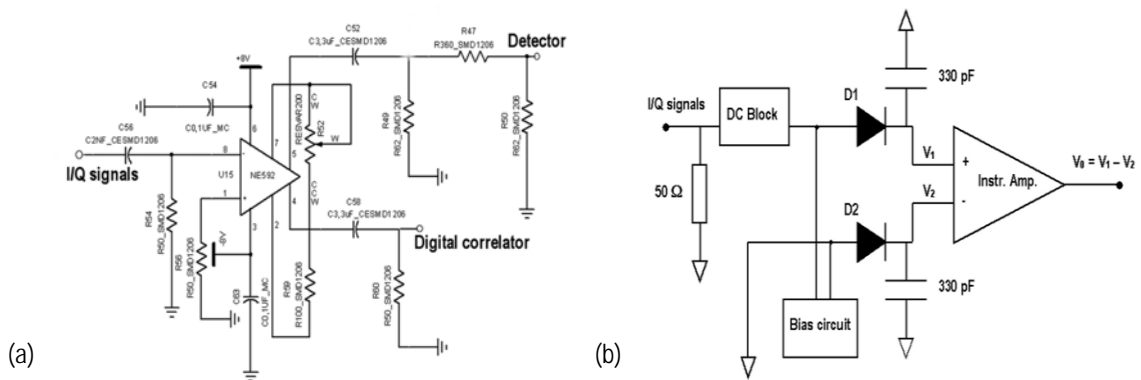

(a)   (b)

Figure 2.18. (a) Video amplifier schematic, and (b) power detector block, [10].

(a)   (b)
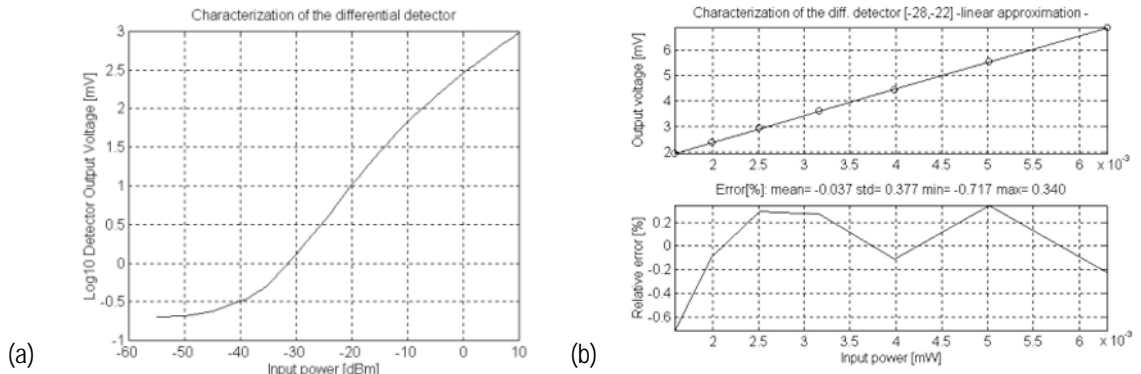
Figure 2.19. (a) Differential detector: V_{OUT} vs P_{IN} curve, and (b) linear range in the differential detector, [10].

The switching rate of the Dicke switch must be much higher than the highest significant frequency in the system-gain variation spectrum, which it is assumed to be 10 Hz [1], and much smaller than the switching time of the video amplifiers [10]. The LF generator synthesizes a square waveform at the switching frequency of the Dicke switch (f_s), with a 50 % duty cycle. A 2 MHz external crystal is used as oscillator and connected to a 74HC4060 to generate a very stable clock signal whose values can be externally selected between f_s = 122 Hz, (selected value), 244 Hz, 488 Hz, 976 Hz, and 1.953 kHz. The maximum f_s selection is selected based on the expression [1]:

$$2 \cdot \frac{\tau_{SW}}{T_S} = 10^{-2} \ , \tag{2.6}$$

where τ_{SW} is the switching time of the Dicke switch from one position to the other one. In this case, the temperature relative error at the Dicke integrator output is 0.5 %.

By observing Figure 2.19 the detector's output is a low voltage (2mV to 6 mV). Hence, after detection a chain of amplifiers are required, with a global gain between 1000 and 10000 depending on the sensitivity, the operation point of the diode, and the saturation point of the amplifier. On the other hand, to maintain the waveform signal, the amplifiers bandwidth has to be as high as possible.

The LAURA's chain gain amplifier is 2200, and it is formed by two operational amplifiers (OP37) with a high gain-bandwidth product (63 MHz), low temperature drift, and low input noise voltage. The lower cut-off frequency (f_{c1}) of the LF band pass filter is chosen to 3 Hz, to eliminate the gain fluctuations. The upper cut-off frequency (f_{c2}) is selected to 80 KHz, considering the LF amplifier's overall response and the OA's transient response. The rise time (t_r, 10 % to 90 %) of a first order low pass filter is expressed as eqn. (2.7) [1]:

$$t_r = 2 \cdot ln(3 \cdot \tau_2) \ , \tag{2.7}$$

where t_r (coincides with τ_{SW}, and τ_2 is the inverse of the cut-off frequency (ω_{c2}).

By combining eqns. (2.6) and (2.7), an expression for $f_{S_{max}}$ is [11]:

$$f_{S_{max}} = \frac{2ln(3) \cdot f_{c2}}{0.5 \cdot 10^{-2} \cdot 2\pi} = 1.2 \, KHz . \tag{2.8}$$

The synchronous detector transforms the square wave from the LF amplifier into DC signals. The clock signal attacks the analog switches used to demodulate the signal and obtain an output voltage proportional to ($T_{ref} - T_A$). The last block of the chain is an analog integrator ($\tau = 1$s), necessary to improve the radiometric sensitivity in this application.

II.1.2 Digital Correlator Unit (DCU)

A complex correlator is used to measure the third and fourth Stokes parameters $U = 2\Re e[E_v \cdot E_h^*]$ and $V = 2\Im m[E_v \cdot E_h^*]$. In Figure 2.20a there is a picture of the circuitry, and in Figure 2.20b a DCU's blocks diagram is presented.

The cross-correlations are computed by a 1bit/2level digital correlator unit (1B/2L) designed and implemented by UPC [12]. It is composed by three MAX915 fast and latch comparators (sampler and hold), whose inputs are the *I* signal (i_V) of the *V*- channel, and the *I* and *Q* signals (i_H/q_H) of the H- channel.

The maximum integration time is 65 seconds at a sampling frequency of 66.6 MHz. The 1B/2L DCU operation consists of computing the ratio of counts in which the sign of the two signals is coincident $\left(N_{sign(x)=sign(y)}\right)$ to the total number of counts (N_{Total}).

$$Z_{xy}(0) = \frac{N_{sign(x)=sign(y)}}{N_{Total}}; \ 0 \leq Z_{xy}(0) \leq 1 ,$$

(2.9)

where x is i_V and y is i_H or q_H.

This operation is performed by a NOT-XOR logic gate, and is implemented by an Altera Programmable Logic Device (PLD) [12].

The offset generated by the up-counter (0.5) must be eliminated by software, to obtain the normalized correlation measured ($\rho_{x,y}$), (eqn. (2.10), and eqn. (2.11)):

$$\rho_{i_V,i_H} = 2 \cdot Z_{i_V,i_H} - 1; \ -1 \leq \rho_{i_V,i_H} \leq 1 ,$$

(2.10)

$$\rho_{i_V,q_H} = 2 \cdot Z_{i_V,q_H} - 1; \ -1 \leq \rho_{i_V,q_H} \leq 1 .$$

(2.11)

For the relationship between the normalized correlation $\mu_{i_V i_H} + j \mu_{i_V q_H}$ and $\rho_{x,y}$ in a DCU 1B/2L is denoted in eqn. (2.12) and eqn. (2.13):

$$\mu_{i_V i_H} = sin\left(\frac{\pi}{2} \cdot \rho_{i_V i_H}\right) ,$$

(2.12)

$$\mu_{i_V q_H} = sin\left(\frac{\pi}{2} \cdot \rho_{i_V q_H}\right) .$$

(2.13)

Finally, after phase calibration by injecting correlated noise, the third (U) and fourth (V) Stokes parameters can be computed from eqn. (2.14) and eqn. (2.15).

$$U = 2 \cdot \sqrt{(T_H + T_{R1}) \cdot (T_V + T_{R2})} \cdot \mu_{i_V i_H} ,$$

(2.14)

$$V = 2 \cdot \sqrt{(T_H + T_{R1}) \cdot (T_V + T_{R2})} \cdot \mu_{i_V q_H} .$$

(2.15)

where: T_{R1}, T_{R2} are the receivers noise temperatures computed with the Friis expression, and T_H, T_V are the average antenna temperatures, measured by the Dicke radiometers.

The correlation radiometer errors that have to be taken into account are:

- offset errors originated from 1B/2L comparator's threshold errors, and oscillators' thermal noise present over the RF band that leaks through the mixers,

- in-phase and quadrature phase errors, originated by mismatches in the channels' frequency response, by demodulators' phase errors, by the different phase of the local oscillator signals arriving at each RF mixer. Errors in the sampling times in the comparators between the i and q channels of the 1B/2L digital correlator.

- amplitude errors (eqns. (2.14) and (2.15)) originated by errors in the estimation of the receivers noise temperature, and mismatches in the channels' frequency response.
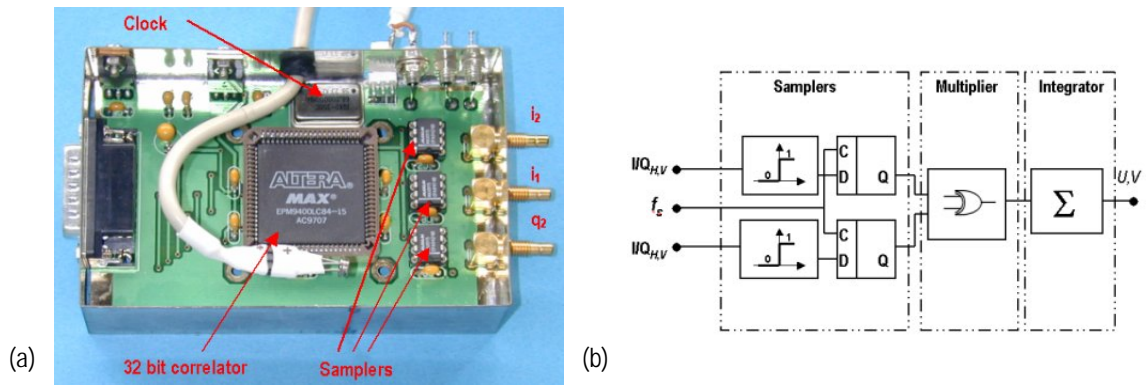

Figure 2.20. Digital correlator radiometer: (a) circuit board, and (b) schematic block diagram.

II.1.3 Additional circuitry

II.1.3.1 Signal conditioning circuit (V_H, V_V, T_{refH}, T_{refV})

The signal conditioning circuit [13] is shown in Figure 2.21a. The voltages associated to the horizontal and vertical brightness temperatures (V_H and V_V) are modified to adjust them to the AD converter range. Four temperatures: H- channel, V- channel temperature references (T_{refH}, T_{refV}), and the LAURA's internal and external temperature signals (T_{int}, T_{ext}) are also adjusted in this module. The four temperatures are calibrated. The linear relationship between the temperatures and the voltage values are summarized in eqns. (2.16) to (2.19).

$$T_{refH}(^{\circ}C) = 31.993 \cdot 10^{-3} \cdot V_{refH}[mV] - 159.63 \cdot 10^{-3} \quad , \qquad (2.16)$$

$$T_{refV}(^{\circ}C) = 31.286 \cdot 10^{-3} \cdot V_{refV}[mV] + 481.63 \cdot 10^{-3} \quad , \qquad (2.17)$$

$$T_{int}(^{\circ}C) = 31.235 \cdot 10^{-3} \cdot V_{int}[mV] + 69.737 \cdot 10^{-3} \quad , \qquad (2.18)$$

$$T_{ext}(^{\circ}C) = 32.404 \cdot 10^{-3} \cdot V_{ext}[mV] - 715.87 \cdot 10^{-3} \quad , \qquad (2.19)$$

An NG4 Seika (± 70º range, resolution 0.01º) analog clinometer (Figure 2.21b), installed behind radiometer is used to acquire the incidence angle, and its output is adjusted and connected to the AD converter as well. The linear relationship between the incidence angle and the voltage is expressed in eqn. (2.20).

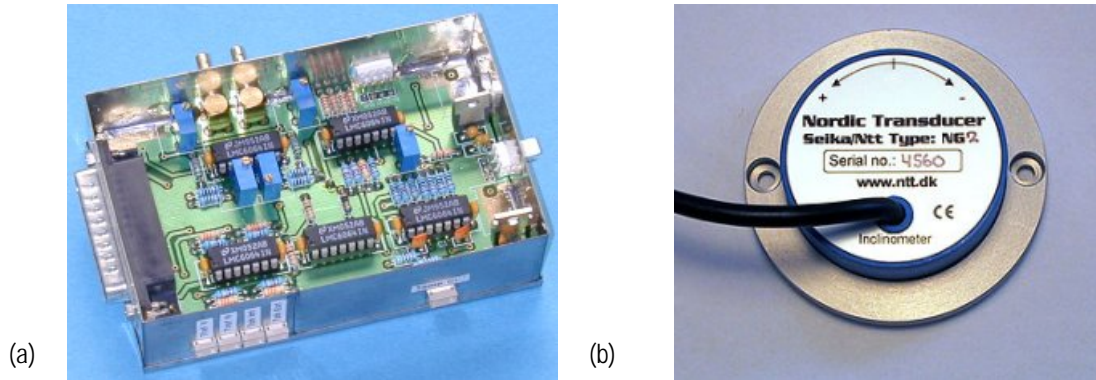$$\theta_i = 78.86 + 37.36 \cdot V_{ADC}[V]. \tag{2.20}$$

Figure 2.21. (a) Signal conditioning circuitry, and (b) clinometer view.

II.1.3.2 AD converter and voltage to current converter unit

A PicoLog ADC-16 high resolution data logger (Figure 2.22a) with eight analog inputs, RS232 output, a 16 bits maximum resolution plus sign, maximum sampling rate 200 Hz at 8 bits per channel, 0.1% accuracy and 0.003 % linearity is used to digitalize the output voltages of the two radiometer channels, four temperature sensors and the clinometer signals. The voltage to current converter unit module (standard RS422, Figure 2.22b) converts the PicoLog ADC-16 RS232 "levels" to TTL "levels" using the Maxim's MAX238 chip.
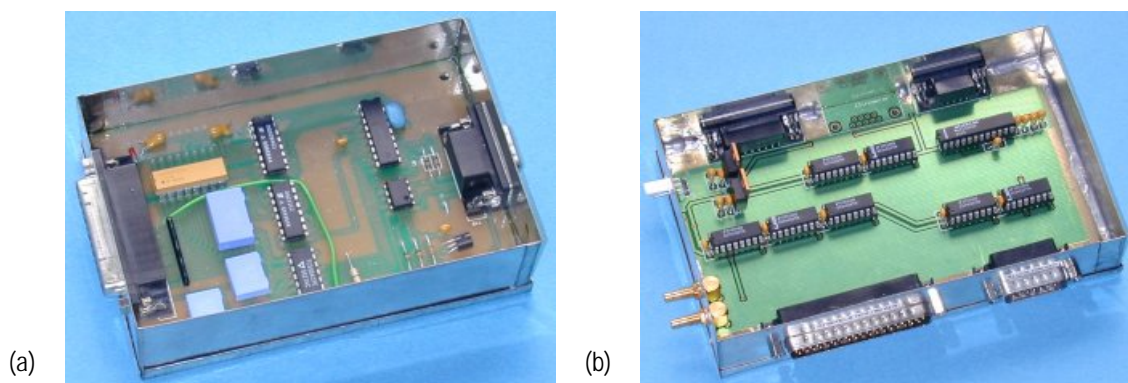

Figure 2.22. (a) PicoLog ADC-16, and (b) voltage to current converter unit module.

The Maxim's MAX238 and the digital correlator unit (DCU) outputs are converted from TTL levels into current signals (National Semiconductor's DS34C87T chip) to improve transmission quality and protection with respect to interferences, since LAURA was designed to operate in a hard industrial environment (Casablanca oil rig).

II.2   Control Unit (CU)

II.2.1 Introduction

The information collected by the LAURA instrument is sent to the LAURA's control unit (CU) (Figure 2.23). The CU is composed by: the Uninterruptible Power Supply (UPS), the step motor controllers, the thermal control unit, the fans unit, the frequency synthesizer (LO), and the industrial PC designed for rough environments.
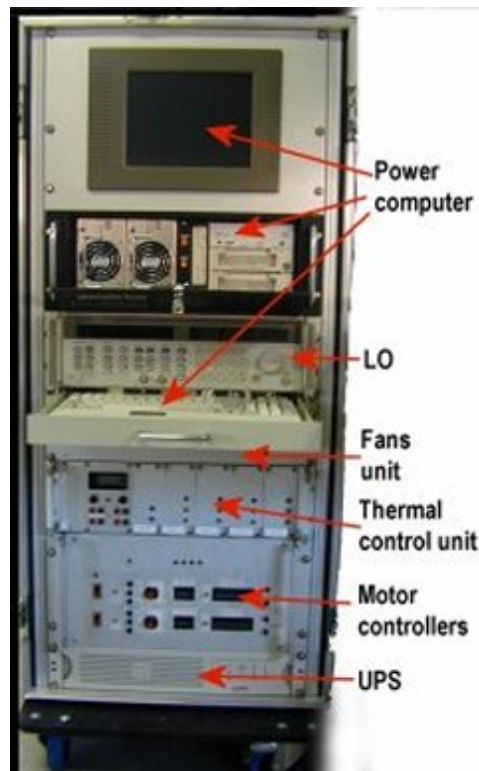

Figure 2.23. Control Unit.

II.2.2 Uninterruptible Power Supply (UPS)

Taking into account the difficulty of the electrical conditions, specially in the WISE field experiments in the Casablanca oil rig, some instruments as the PC, the frequency synthesizer, the motor controllers, and the radiometers were fed by an on line UPS from APC, with a maximum power of 1,000 VA. The UPS is controlled by software via the serial port, using the PowerChute application for Windows.

II.2.3 Motor controller (MC)

The LAURA radiometer was mounted on a 0º - 360º azimuth and $\pm$ 90º zenith scanning stainless steel positionner. During the WISE field experiments it was installed on a custom built terrace at 33 m above the sea surface, and during FROG field experiment and at 2 m height, pointing to a foam-covered 3 m x 7 m pool.

27

Figure 2.24. Motor controllers.

The scanning was performed by two step-motors, manually or software controlled, using two Slow-Syn 330 pix controllers (Figure 2.24). The electrical specifications are: AC voltage 220 V @50 Hz, AC current 0.5 A. The step rate range is from 0 to 10,000 half steps per second, being half step the driver step resolution. The number of steps is 400 in a 360° range. Motor specifications are explained in the positioning system section.

II.2.4 Thermal control unit (TCU)

Since the radiometer's accuracy depends on the thermal stability, it has to be thermally controlled. A thermal control unit has been implemented. There are two different temperature control systems that will be explained in the following points. For the WISE field experiments a simpler analog temperature control was used. It is based on a proportional control, and it is totally implemented by hardware. For the FROG experiment a second and more sophisticated temperature control was implemented. It is developed by software, and hence the main parameters can be controlled.

II.2.4.1 Analog temperature control

The physical temperature (T_o) contributes to the behavior of any electronic circuit. According to [10], T_o variations (ΔT_o) affect T_A', and create low frequency gain fluctuations of the radiometer front-end. On the other hand, and due to the size of the instrument (0.3 m³), it is possible to correct the output fluctuations due to the ΔT_o [10], although it is complicated to characterize the instrument's temperature response, because the time constants between the points where noise is created, and the points where the temperature sensors are mounted. Finally, the smaller the temperature difference between the antenna and the front end, the higher stability of the measurements is produced. For this reason LAURA's antenna is placed in front of the receiver and inside of the thermally controlled box. The selected T_{ref} must be higher (or lower) than the maximum (or minimum) measured T_A to avoid ambiguities. Obviously the selected option is the first one, because in the Dicke calibration process, the selected cold load will be the

sky (~ 6 K). LAURA is designed to measure the ocean salinity and the soil moisture. The maximum T_A considered is 313 K, so T_{ref} will be higher than this value, and hence a heating system is required, (except during the day time in the summer seasons). The LAURA's analog control system consists of keeping the reference load and the front-end are at the same temperature. In this situation, the reference load thermal isolation is not required, being the circuitry simpler. However, the higher the front-end's T_{REC} the lower Dicke radiometer sensitivity is.

The Dicke radiometer is thermally controlled at T_{ref} = 45 ºC [10] and [14]. A set of pictures of the temperature control instrument are shown from Figure 2.25a to Figure 2.25c. It is composed by a proportional temperature control module, and four independent switching power supplies to drive eight thermoelectric coolers (TECs). An automatic hysteresis proportional control was implemented using LM35 temperature sensors located in different places of the radiometer, one per channel (reference temperature) to heat or cool the radiometer. TCU supports two operating modes. The first mode to heat the instrument quickly, and the second one - automatic mode - to fine control the temperature of the instrument. The maximum power rating is about 800 W.
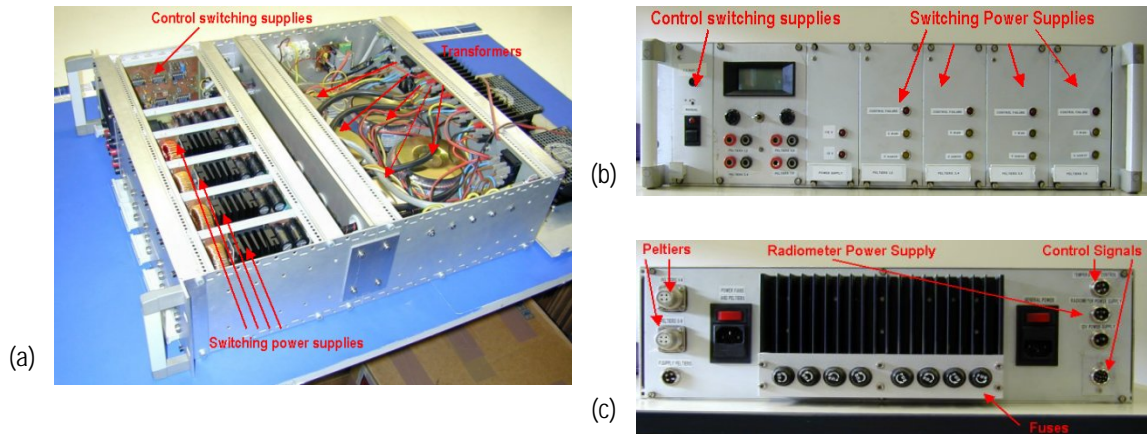

Figure 2.25. LAURA's control temperature instrument. (a) General aspect, (b) front view, and (c) rear view.

The control temperature board is presented on Figure 2.26a, and its block diagram in Figure 2.26b. First of all, a current proportional to the LAURA instrument average temperature measured by the LM35 sensors attacks the instrumentation amplifier to make the current/voltage conversion, and to increase the input signal range by a 10 factor (G = 10). The control signal (C$_2$) is generated from a reference voltage (~4.5V), and attacks the mechanical switch to invert the Peltier's cells (TECs) polarity, if necessary. When C$_2$ is off, the current temperature of the radiometer is lower than T_{ref}, and the thermoelectric cooler heats the radiometer. The histeresys cycle (ΔH_v) in volts is about 10.16 mV, and is fixed by two linear resistors (100 Ω, and 113K Ω) and the LM6064 operational amplifier (comparator). Its value is computed as in the eqn. (2.21):

$$\left| \Delta H_V \right| = \left(V^+ - V^- \right) \cdot \frac{100}{113K + 100} \quad , \tag{2.21}$$

where V^+ and V^- are the amplifier power supplies (+6.5 V, -5 V), respectively, and its corresponding (ΔH_T) in °C is computing by the following expression (eqn. (2.22)) :

$$|\Delta H_T| = \frac{|\Delta H_v|}{LM35\left(mV/_{\circ C}\right) \cdot G} \quad , \tag{2.22}$$

where $LM35\left(mV/_{\circ C}\right)$ is the LM35 voltage/temperature ratio, which is 10, and G is the instrumentation amplifier's gain. The equivalent histeresys is about 0.1°C.

With the purpose of avoiding the mechanical switch damage (switching numbers are limited 150,000), and assuming that C_2 is almost always off, two additional histeresys comparators with a reference level beneath ($\sim$44.5 °C) and above ($\sim$45.5°C) from T_{ref} are used. When the radiometer's current temperature is close to T_{ref}, two additional circuits (depending if the radiometer's current temperature is lower or higher than T_{ref}), modify the V_{SENSOR} signal, decreasing the current through the Peltier's cells. From the comparator outputs, two control signals are generated (C_1 and C_3), to attack the analog switches (CD4066), which inputs are the original or the modified V_{SENSOR} signal. At the end of the switches and conditioning circuits, a reference level (PWM$_{IN}$) is generated. Its range of values oscillates between -3.5 V to 0.5 V, depending on the amount of current through the Peltier's cells.

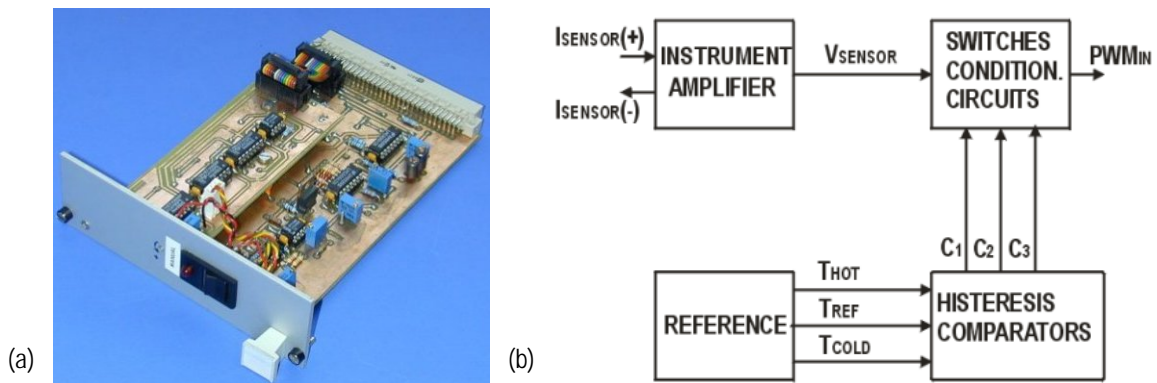(a)   (b)

Figure 2.26. Temperature control module (a) view, and (b) block diagram.

The switching supply board is presented in the Figure 2.27a.

There are four identical modules. Each module feeds a pair of Peltier's cells and is composed by the following blocks:

- the buffer circuit to feed appropriately the fourth PWM generators,

- the pulse wave modulator that it is generated by the NE5561 device. It is a specific control circuit for use in switch-mode power supplies composed by a temperature-compensated power supply, a PWM, a saw-tooth oscillator, and the output stage. A square pulse (± 5V),

with a variable duty cycle between 10 % to 90 %, needed to attack the switching driver, is generated at the NE5561 output by injecting the PWM_{IN} signal.

- the offset pulse block is designed to conditioning the signal levels at the output of the PWM generator to attack appropriately the MOSFET gate (0 V to saturate or VSS to turn off the MOSFET).

- the driver is a step-down switching power, composed by an enhancement n-MOSFET (STP10NA40), maximum drain current 10 A and high speed switching. VDD and VSS voltages are approximately +15 V and –15 V respectively. Maximum voltage applied over the load is VDD-VSS,

- to avoid power supply instabilities, a feedback circuit is implemented. The signal at the feedback circuit output is compared to the PWM_{IN} signal related to the radiometer's temperature, and the result (error) subtracted from the original PWM_{IN}.

(a)   (b)
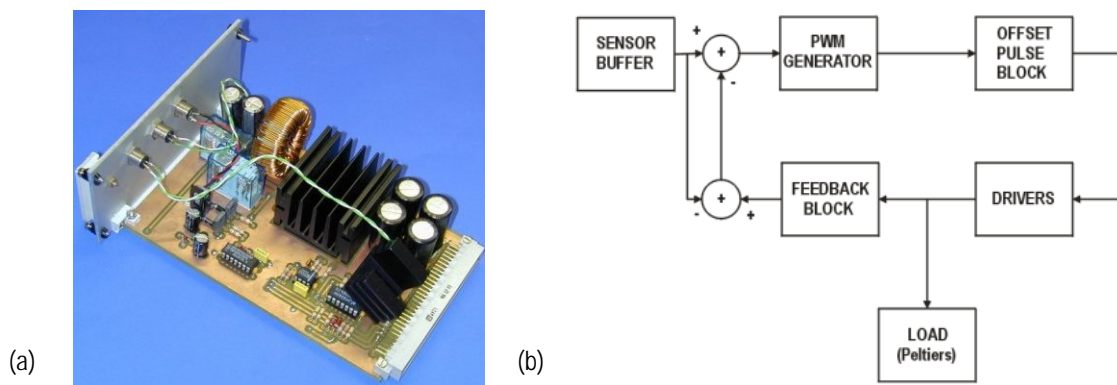
Figure 2.27. Switching supply module, (a) view, and (b) block diagram.

Eight pairs of fans and heatsinks (eight inside and eight outside) are used to mount the TECs as seen in Figure 2.28. TECs devices can heat or cool the radiometer depending on the external conditions. It is normally necessary to heat the radiometer. However in warm places during day, it can be necessary to cool it. Other advantages to use TECs are: they are a solid state devices with high thermal stability ($\pm$ 0.1º), and there are no vibrations. The whole radiometer is mounted behind the antenna inside a plastic structure (high molecular weigh poly-ethylene), wrapped internally with a metal film to prevent radio-frequency interferences. A thin layer of polystyrene is used as a radome and at the same time preserves the instrument of external humidity, and isolates it from external temperature changes. The radiometer power supply is mounted in the thermal control unit, electrically isolated from the switching power supplies using the infineon technologies linear optocoupler (IL300).
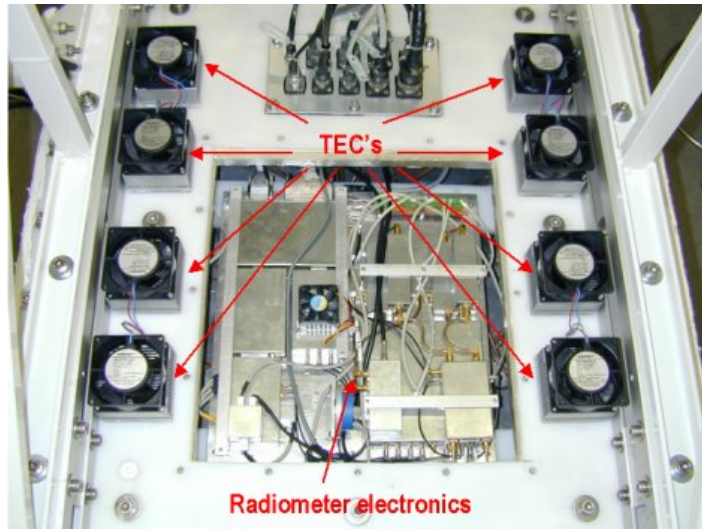
Figure 2.28. Radiometer rear view aspect, showing the 8 TEC modules temperature to heat/cool the radiometer.

Figure 2.29a and Figure 2.29b present a sample of the instantaneous reference load and external temperatures measured during 1 hour during the WISE field experiment. First of all, the T_{ref} is relatively well controlled in a 0.14 °C range of values, in front of the T_{ext} variations (3 °C). Second, there is a dependence of the external temperature inside of the radiometer, with an elapsed time of ~150 sec due to the instrument isolation and the proportional temperature control.
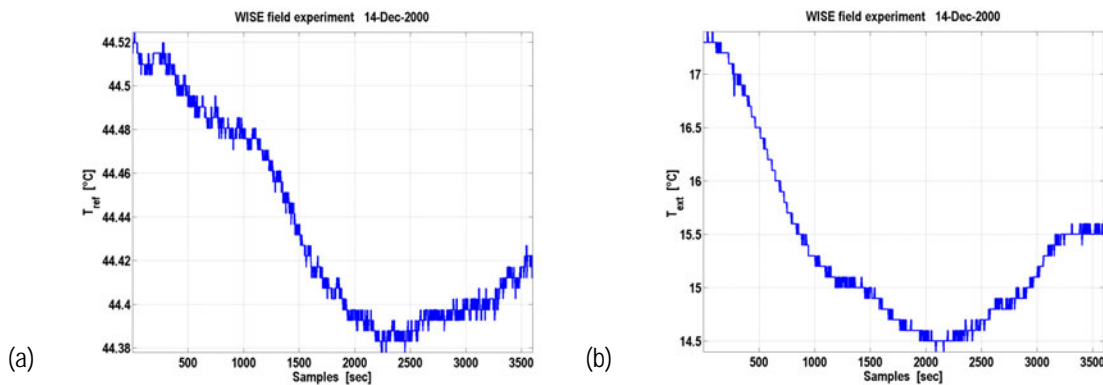

(a)   (b)

Figure 2.29. (a) Instantaneous internal reference load temperature and, (b) instantaneous external temperature of the WISE field experiment.

II.2.4.2 The software temperature control

To minimize the external temperature dependence and to integrate the thermal and the radiometric measurements using the same interface, a software control temperature was also implemented. The main advantages are: the possibility of implementing a more sophisticated proportional, integrate, and derivative temperature control (PID), and the flexibility in front of the hardware system because the PID parameters can be selected by the user.

II.2.4.2.1   Basic concepts on classic control theory

The block diagram of a typical control system is presented in Figure 2.30. The main function of $G_c(s)$ is processing and minimizing the error signal $E(s)$, and attack properly the system $G(s)$ to achieve the specific requirements.
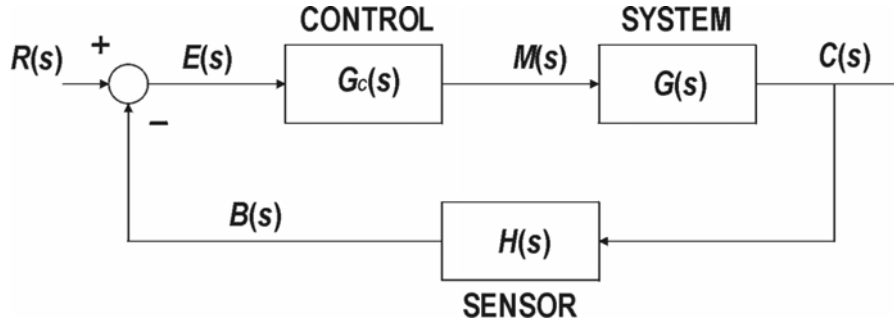

Figure 2.30. Blocks diagram of the basic control system. Block $G_c(s)$ is the control System, $G(s)$ is the system to be controlled, and $H(s)$ the sensors.

There are basically four types of control systems to get this:

II.2.4.2.1.1   Proportional control (P)

The signal at the output of $G_c(s)$ is proportional to the error signal $E(s)$, according to the next expression:

$$M(s) = k_p \cdot E(s) ,\qquad(2.23)$$

where:

- $M(s)$ is the Laplace transform of the control signal,

- $E(s)$ is the Laplace transform of the error signal, and

- k_p is the proportional sensitivity.

According to Figure 2.30, the stationary response of the error signal (e_{ss}) when $R(s) = 1/s$ is expressed:

$$e_{ss} = \lim_{s \to 0} \frac{1}{1 + G_c(s) \cdot G(s) \cdot H(s)} ,\qquad(2.24)$$

hence, the proportional sensitivity can be written as:

$$K_p = \lim_{s \to 0} G_c(s) \cdot G(s) \cdot H(s)\qquad(2.25)$$

The key of the control system is to analyze the stationary error depending on the input. The main advantage of the P control is the simplicity of the circuitry. On the other hand, if an integrator element does

not exist, a residual stationary error is present all the time. Finally, there is a compromise between the minimum transient response and the system stability. This type of control was developed for the WISE 2000 and 2001 field experiments to control thermally the instrument.

II.2.4.2.1.2 Proportional Integrate control (PI)

The signal at the output of $G_c(s)$ is proportional to the integrate of the error signal $E(s)$, according to the expression:

$$M(s) = k \cdot \left(1 + \frac{1}{T_i \cdot s}\right) \cdot E(s),$$ (2.26)

where T_i is the integration time,

The PI control considers an integral element and, consequently a pole (s = 0) is added in the transfer function. The main advantage is the full elimination of the stationary error. The disadvantage of these types of systems is the instability due to the new pole added. The proportional control minimizes this effect.

II.2.4.2.1.3 Proportional Derivative control (PD)

The signal at the output of $G_c(s)$ is proportional to the derivate of the error signal $E(s)$, according to the expression:

$$M(s) = k \cdot \left(1 + T_d \cdot s\right) \cdot E(s),$$ (2.27)

where T_d is the derivative time.

The principal advantage of knowing the derivate of the error signal, it is the prediction of the dynamic behavior of the signal. In other words, an excessive increase of the error signal can be controlled "*a priori*", increasing the stability of the system. However the stationary response is never achieved, using only the derivative action.

II.2.4.2.1.4 Proportional Derivate Integral control (PID)

The PID control is the combination of the types of controls explained before. $M(s)$ depends on the error signal $E(s)$ and the three proportional constants (k, T_d and T_i), and can be expressed as:

$$M(s) = k \cdot \left(1 + T_d \cdot s + \frac{1}{T_i \cdot s}\right) \cdot E(s),$$ (2.28)

The principal consequences are: the minimization of the stationary error due to the integrative effect, and the stability of the system due to the derivative action that permits to reduce the transient response.

During the preparation to FROG field experiment a PID control was implemented to further improve the instrument's temperature control. The PID control is implemented by software, and its output is digital-to-analog converted, using an input/output card 8255 I/O, and a AD767 12 bits DAC (Figure 2.31a). DAC's output is available when the asynchronous chip select (CS) signals is selected. Furthermore, the hardware control (Figure 2.31b) is kept, and it can be switched on by selecting the HARD/SOFT signal. The HARD/SOFT signal evolution depends on:

- the asynchronous disable or enable analog signal (D/E: D/E = 0, analog control is activated),

- the watchdog, programmed on the 8255 I/O timers according with the function table, Table 2.5.

The HOT/COLD asynchronous signal indicates if the radiometer has to be heated or cooled.

Table 2.5. Analog or software temperature control (HARD/ SOFT). Function table

Watchdog output (10 sec)	D/E	HARD/SOFT
0	0	0
0	1	1
1	0	0
1	1	0

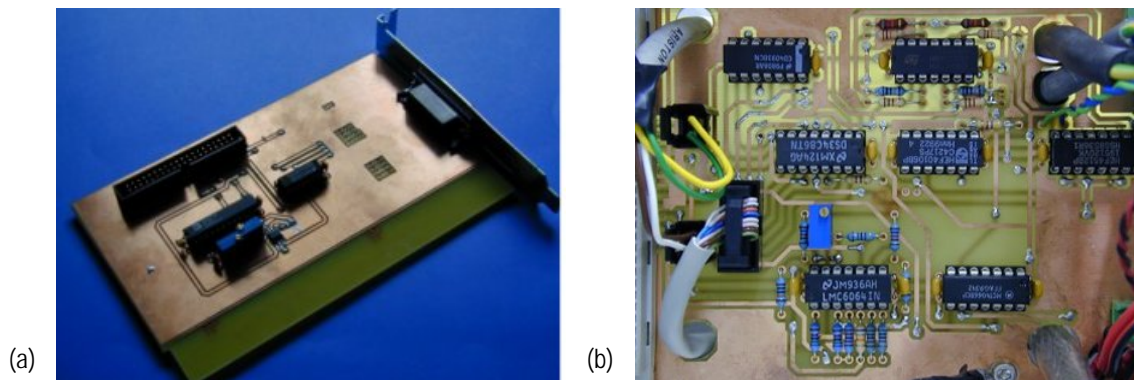(a)   (b)

Figure 2.31. (a) Digital to analog converter board to connect to the 8255 I/O card, prepared to be install on a ISA bus socket, and (b) circuitry to switch the analogical and the software temperature control.

The PID constants (k, T_d, and T_i) are programmed by software and depend on some parameters as:

- instrument's thermal inertia,

- the temperature difference between the radiometer ($\sim 45°C$) and the environment, and

- the external temperature variations.

The PID constants were programmed using a trial and error method, according to the parameters mentioned before. Values are summarized in the next table:

Table 2.6. Empirical PID constants

k	15
Td	0.05
Ti	0.005

In Figure 2.32a and Figure 2.32b the instantaneous reference load and external temperatures are presented. The instrument is mounted inside of the anechoic chamber to analyze the radiometer's thermal behavior. By observing the instantaneous data sequence (~15 hours), the thermal deviation is bellow 0.01 K with an external temperature variation of 0.35 K. In Figure 2.32c and Figure 2.32d the instantaneous reference load and, external temperature measured during 1 hour in the IRTA facilities (FROG field experiment) are presented. The variations of the reference temperature ΔT_{ref} are about 0.08 °C, when the external temperature variations ΔT_{ext} are higher than 3.5 °C, (more than 1 hour of measurements).
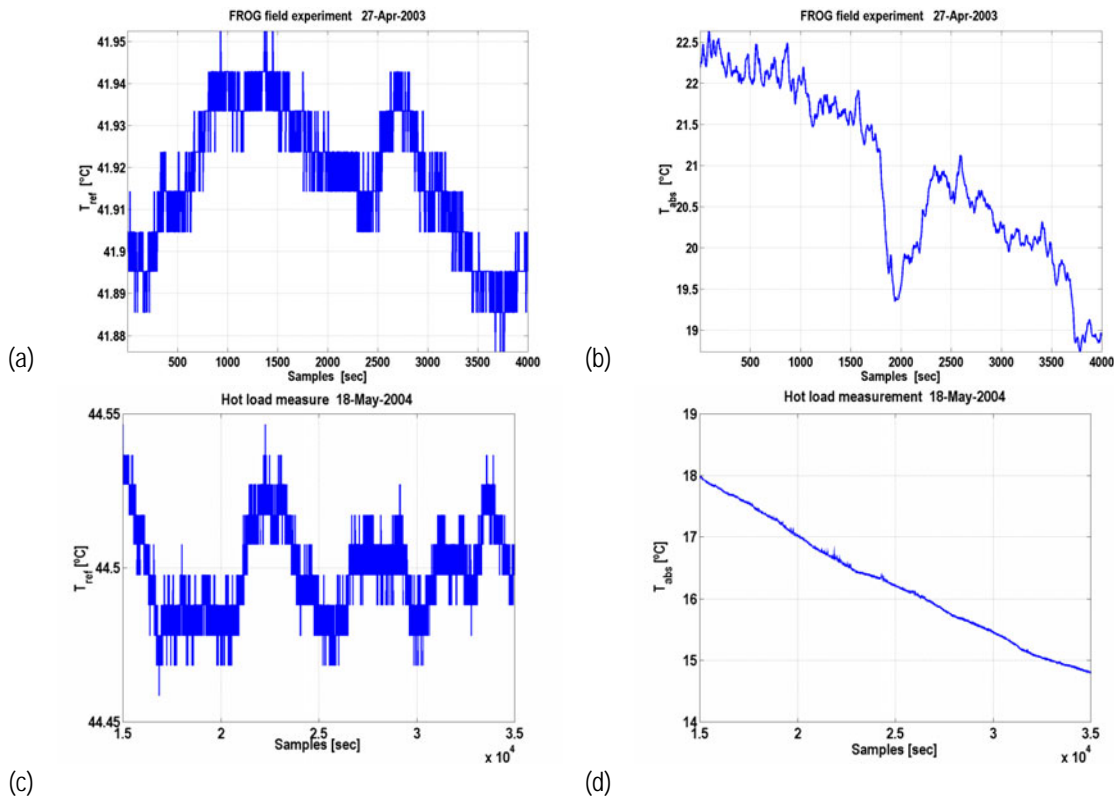

Figure 2.32. Instantaneous reference load temperature (a) FROG field experiment and, (b) hot load measurement and, instantaneous external temperature (c) the FROG field experiment and, (d) hot load measurement.

II.2.5 Fans unit, frequency synthesizer and power computer

Above the TCU, a unit of 3 fans (AC fed) ventilates the heatsinks of the switching power supplies. A –10 dBm power level 1.413 GHz frequency tone is generated using the frequency synthesized sweeper HP-83752B as LO as an alternative option to the PLL local oscillator.

Radiometric and meteorological data are collected by an industrial PC designed for extreme conditions, (Figure 2.33a and Figure 2.33b). It is composed by: two independent power supplies, two

portable hard disks, a CD recorder unit, a floppy disk and a flat LCD monitor. Other characteristics are: Pentium III processor (500 MHz), 256 MBytes SDR, 16 ISA bus slots, 4 PCI bus slots. Additionally several temperature and humidity sensors are located inside the PC to test and control the environment conditions.

An additional slot of ISA cards is necessary to control the instrument. Some of them have already been described as:

- the 8255 I/O card to control the digital correlator asynchronous signals, and the temperature control signals,

- the digital-to-analog convert card to generate the signal to attack the *Peltiers'* power supplies,

- a current to voltage (TTL levels) converter card related to the digital correlator signals, (Figure 2.34a), and

- a current to voltage (RS232) converter card to acquire the ADC-16 data (Figure 2.34b).

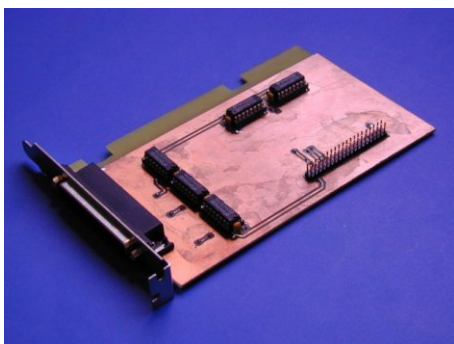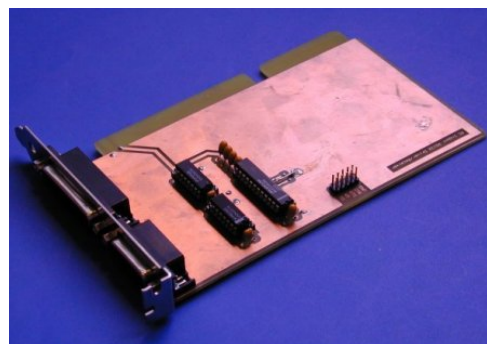(a)   (b)

Figure 2.33. Industrial PC, (a) front view, and (b) rear view.

(a)   (b)

Figure 2.34. Current to voltage converters, (a) digital correlator signals, and (b) PicoLog ADC-16.

II.3   The positionner system

The LAURA instrument is mounted on a stainless steel hollow cylindrical pedestal, as it can be seen in Figure 2.35a and Figure 2.35b. An inverted stainless steel U is on the top of the pedestal to allow the azimuth movements. Plastic box receiver is screwed into a triangle structure, which pivots over the

inverted U to achieve the incidence movements. To balance the LAURA's weight (60 Kg) a set of lead disks are mounted as counterweights. The cables that are connected to the instrument pass through the hollow pedestal.

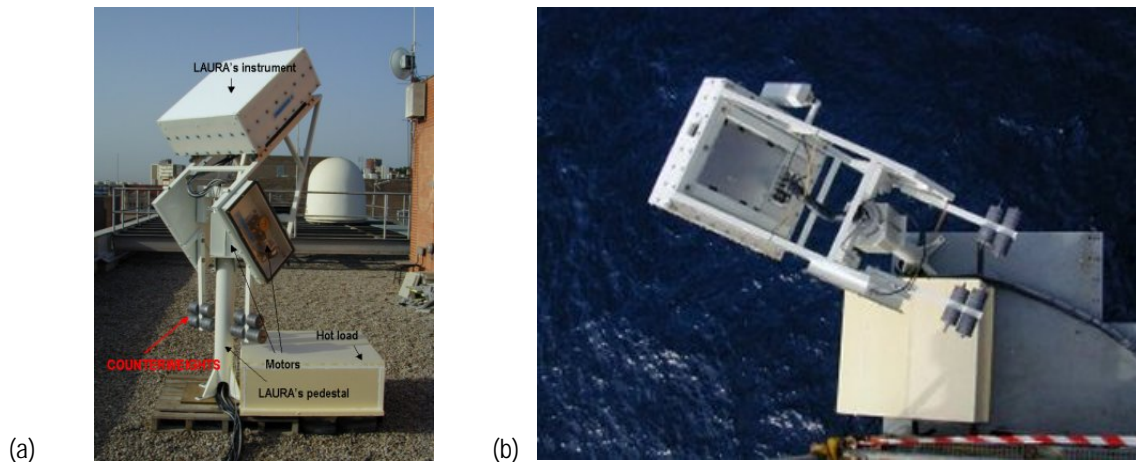(a)   (b)

Figure 2.35. LAURA radiometer mounted on the pedestal, (a) at UPC facilities during testing, and (b) at the Casablanca oil rig during WISE 2001.

To move the radiometer, two Sanyo Denki step-motors are used. Figure 2.36a shows a picture of the elevation motor. A gear-reduction system (1÷750) is necessary, to overcome the radiometers weight and the wind loads. The azimuth movement is achieved using a second motor placed inside of the pedestal, Figure 2.36b, with a reduction of 1÷75. The Sanyo Denki motor resolution (no gear-reductions is accounted) is 0.45°. The boundary azimuth and elevation movements are controlled by a set of micro switch levers.
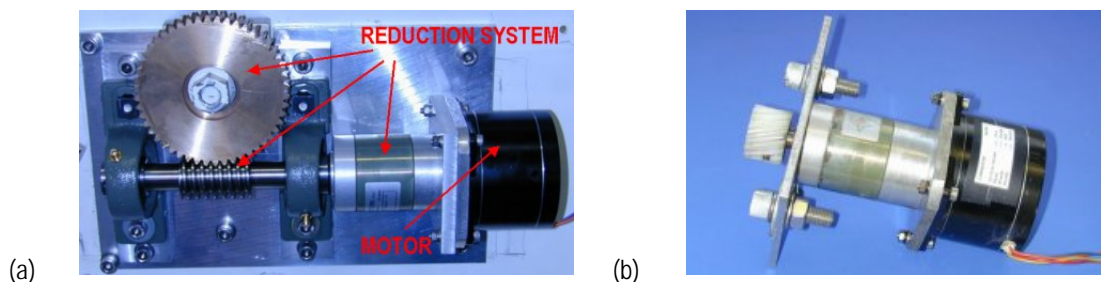

(a)   (b)

Figure 2.36. Radiometer movement system, (a) elevation motor, and (b) azimuth motor.

II.4   Other instruments

II.4.1 Meteorological station and GPS receiver

A meteorological station kit from Fascinating Electronics (Figure 2.37a and Figure 2.37b) provided rain rate, wind speed and direction, atmospheric pressure, relative humidity (2 sensors), and temperature (5 sensors) measurements. This instrument was connected to the same computer as the radiometer through a RS232 interface. Meteorological data were time-tagged with the Garmin GPS time, and saved in the same files than the raw Stokes elements vector. These data were used in the numerical models to

estimate the atmospheric effects in the down-welling atmospheric radiation. An specific software developed by Fascinating Electronics provides the set of meteorological data which will be read by the LAURA's control routines [15] using Dynamic Data Exchange (DDE libraries).
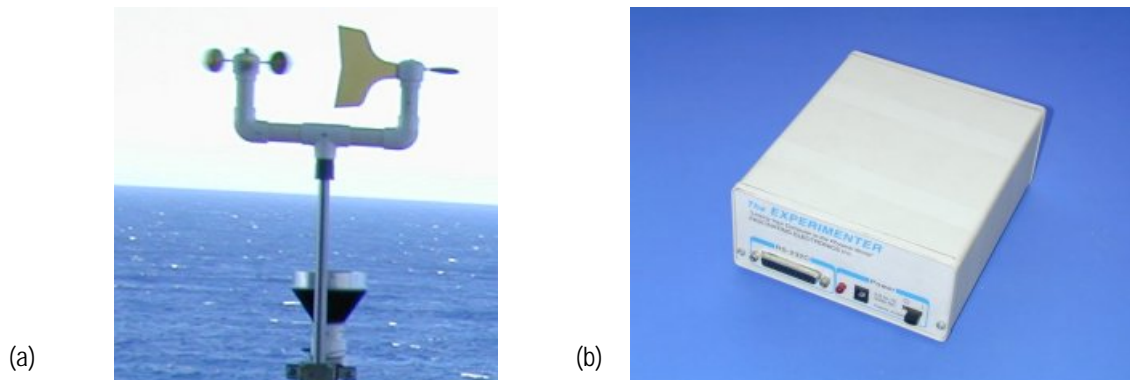
(a)   (b)

Figure 2.37. (a) Meteorological station, and (b) meteorological station unit.

II.4.2 Video cameras

During the WISE field experiments a video camera (model Ultrak KC550xCP) with 512x582 pixels and a 8.5 mm lens, auto-iris and 35.6°x25.2° field of view was mounted on the L-band radiometer pedestal as shown in Figure 2.38a. During the FROG field experiment the ULTRAK video camera was used in a periscope to measure foam vertical profiles, and a second video camera (model SONY SSC-DC393, Figure 2.38b), with 752x582 pixels was mounted on the L-band radiometer. The analysis of the images restricted to a 20° field of view (coincident with the antenna beamwidth) was used to:

- estimate the sea foam emissivity by comparing the instantaneous sea foam coverage and the instantaneous T_B (T_H and T_V),

- evaluate the water surface foam coverage of the sea surface to try to determine the relationship between foam coverage and wind speed, during the WISE field experiments,

- evaluate the water surface foam coverage artificially generated by pumping air through a net of 104 air diffusers, during the FROG field experiment.

During the FROG campaign, the Ultrak KC550xCP video camera, with a 5-50 mm lens, auto-iris and 5.4°x 4.1° field of view was mounted on a periscope to take foam vertical profile images to study:

- bubbles' radii and their distribution, and

- the foam thickness layer,

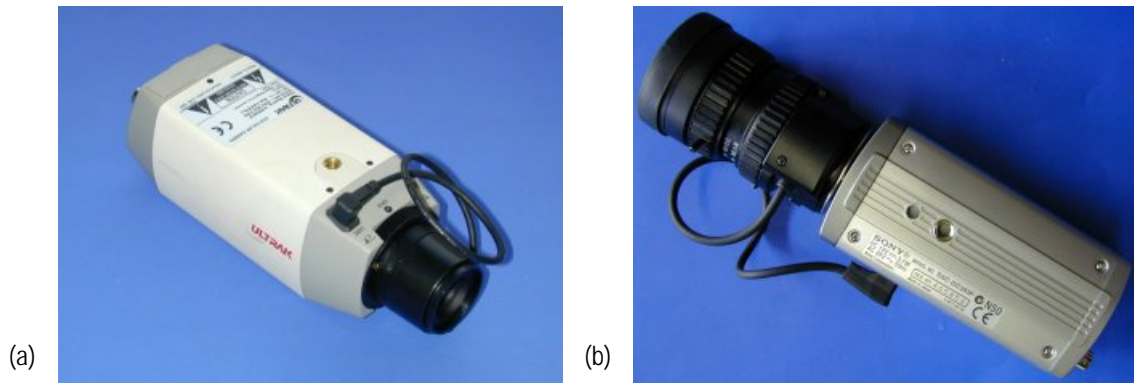in a wide range of salinities for a better understanding of the theoretical models.

Figure 2.38. Video cameras, (a) Ultrak KC550xCP, and (b) SONY SSC-DC393.

II.5   The LAURA's control software

LAURA'S control software was developed to acquire data (radiometric and meteorological data from the ADC-16 and the Fascinating Electronics meteorological station kit) in an automatic manner as specified by the user. The LAURA's routines have been developed to accomplish following goals:

- to read the Picolog ADC-16, and the meteorological data using DDEs,

- to send the instructions to the digital correlator at a specific time,

- to send the asynchronous signals MEAS and CNI to the instruments,

- to send the information to the step by step motor's controller for the azimuth and incidence scanning and,

- to show and save the data.

There are two modes of operation: automatic and manual that can be selected from the Main Control Panel. In the automatic mode of operation input parameters are read from a file with the following sequence:

- cold and hot Dicke calibration, and offset and phase calibration,

- measurement sequence, indicating azimuth and elevation angles and measurement time, and

- final calibration again.

In the manual operation mode it is possible to enter angles and time parameters individually at any time. During the measurement process a graph representation of radiometric data is made, as well as a set of physical parameters as temperature, humidity, wind velocity and direction. LAURA's software main control window, -during the WISE field experiments - is presented in Figure 2.39.
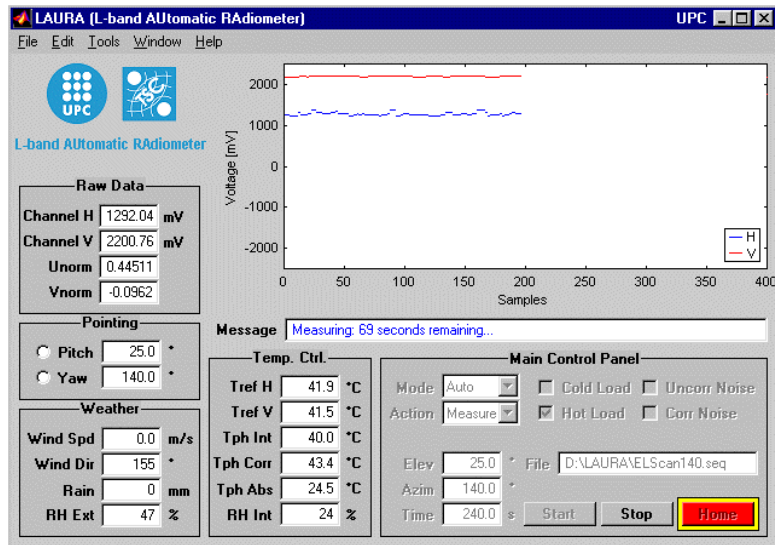
Figure 2.39. WISE LAURA interface.

Since the software temperature control was implemented for the FROG campaign, the LAURA's interface has changed as it can be observed in the Figure 2.40. In the box Mode of the Main Control Panel three possibilities referred to the temperature control can be chosen: a) normal mode, (analogical control temperature is selected), and b) software and PID mode, (software control temperature is on). The PID parameters, (K_p, T_i, and T_d) and the nominal temperature reference can be selected. This mode was used during the FROG field experiments.
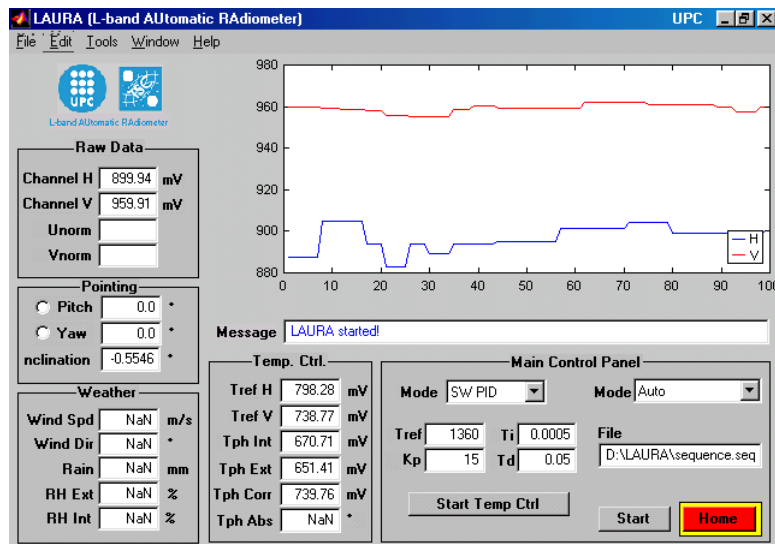

Figure 2.40. FROG LAURA interface.

As a future research line, a neural network can be programmed to minimize the effects that intervene on the PID control parameters, specially the external temperature variations.

II.6   Conclusions

In this chapter a description of the receiver composed by two Dicke radiometers and the digital correlator unit, the thermal temperature control composed by an analog temperature control (WISE field experiments) and a software temperature control (FROG field experiment), the control unit description have been presented.